Article

The Characteristics of Hydrodeoxygenation of Biomass Pyrolysis Oil over Alumina-Supported NiMo Catalysts

Dong-Jin Seo [1,†], Jong Beom Lee [1,†], Yu-Jin Kim [1], Hye-Ryeong Cho [1], So-Yeon Kim [1], Ga-Eun Kim [1], Young-Duk Park [2], Geon-Hee Kim [2], Jung-Chul An [3], Kyeongseok Oh [4,*] and Joo-Il Park [1,*]

[1] Department of Chemical & Biological Engineering, Hanbat National University, Daejeon 34158, Republic of Korea; tjehdwls0963@naver.com (D.-J.S.); whdqja0020@naver.com (J.B.L.); yzzy0840@naver.com (Y.-J.K.); ryeong2829@gmail.com (H.-R.C.); s0s0yeon@naver.com (S.-Y.K.); kenieun@naver.com (G.-E.K.)
[2] Department of Mechanics-Materials Convergence System Engineering, Hanbat National University, Daejeon 34158, Republic of Korea; parkyd@hanbat.ac.kr (Y.-D.P.); ghkim@hanbat.ac.kr (G.-H.K.)
[3] Carbon Materials Research Group, Research Institute of Industrial Science & Technology (RIST), Pohang 37673, Republic of Korea; jcan@rist.re.kr
[4] Department of Chemical & Biological Engineering, Inha Technical College, Incheon 22212, Republic of Korea
[*] Correspondence: kyeongseok.oh@inhatc.ac.kr (K.O.); jipark94@hanbat.ac.kr (J.-I.P.); Tel.: +82-42-821-1530 (J.-I.P.)
[†] These authors contributed equally to this work.

Abstract: The hydrodeoxygenation (HDO) of biomass pyrolysis oil (BPO) was evaluated in the presence of two commercial alumina-supported transition metal catalysts, NiMo/alumina-1 (NM1) and NiMo/alumina-2 (NM2). The study explored two characteristic aspects: how HDO reaction conditions affected the oxygen content, density, and boiling point distribution of BPO with varying temperature and HDO reaction time, and the roles of catalysts. Characterizations of HDO-treated oils included elemental analysis, GC-MS, SIMDIS, ^{13}C NMR, and ^{1}H NMR, and characterizations of catalysts included NH$_3$-TPD, XRF, and TPO-MS analysis. The results show that both NM1 and NM2 catalysts removed oxygenated compounds effectively, which led to decreases in density and shifts toward higher boiling point distributions of BPO. Compared to the NM1 catalyst, NM2 had a higher acidity and enhanced HDO activity. The best HDO reaction performance was achieved in the presence of the NM2 catalyst at 300 °C. Furthermore, HDO reactions showed a significant amount of CO_2, CH_4, C_2H_6, and C_3H_8, which suggests that HDO reactions proceeded via a series of reactions of decarboxylation, water–gas shift, and methanation. In addition, hydrocarbon fraction tests suggested a favorable potential for the blending of HDO-treated biomass pyrolysis oil (HDO-BPO) with petroleum-derived fractions.

Keywords: hydrodeoxygenation; NiMo/alumina; sulfidation; biomass pyrolysis oil (BPO); hydrocarbon fraction test

1. Introduction

Over the past decade, the average concentration of carbon dioxide (CO_2) in the atmosphere has increased by approximately 2.5 ppm, prompting a focus on the development of renewable energy sources aimed at achieving carbon neutrality through the reduction of CO_2 emissions. Among the various strategies available, biomass has garnered considerable attention for its economic potential, allowing for benefits without significant alterations to existing infrastructure [1–3]. Furthermore, the production of BPO (biomass pyrolysis oil) has been found to reduce CO_2 emissions by approximately 80% compared to heavy

oil production, marking it as a promising energy resource from an environmental perspective [4,5]. Lignocellulosic biomass, which comprises cellulose, hemicellulose, and lignin, is a renewable resource capable of generating chemicals and fuels through physical, chemical, and biochemical conversion technologies [6]. Commonly employed conversion methods include combustion, gasification, and thermal pyrolysis. Among these, pyrolysis is notable for its process of thermally decomposing biomass at high temperatures in the absence of oxygen, which provides advantages in terms of operational simplicity and economic efficiency [7]. Additionally, when biomass is pyrolyzed at temperatures between 400 and 800 °C, it yields a liquid form of oil that is convenient for storage and transportation [8].

BPO (biomass pyrolysis oil) can be utilized as a substitute for fossil fuels, as well as a feedstock for various industrial chemicals, including paints, adhesives, and plastics [9]. However, crude BPO is a complex mixture comprised of acids, alcohols, aldehydes, esters, ketones, phenols, and furans. Notably, compounds like furfural, dimethylphenol, 2-methoxy-4-methylphenol, and furanones constitute significant proportions, especially when feedstocks high in lignin content are converted [10]. Meanwhile, crude BPO has a low heating value of 15–19 MJ/kg when compared to the heating value of petroleum (ca. 40 MJ/kg) [8,11]. The polar nature of crude BPO also complicates its blending with non-polar fossil fuels, making it challenging to use without additional additives. During storage, organic components may even polymerize over time, leading to increased viscosity and instability, particularly due to the presence of oxygenated compounds [8,11]. Given these characteristics, crude BPO needs further upgrading processes [4]. Upgrading techniques include a series of hydrodeoxygenation (HDO) reactions, catalytic cracking, steam reforming, molecular modification, the use of supercritical fluids, and esterification [12]. HDO utilizes catalysts under high-pressure hydrogen conditions to convert oxygen-containing compounds such as acids, aldehydes, and alcohols [13]. The HDO reaction can be broken down into four major reactions: hydrogenation of C–O and C–C bonds, dehydration of C–OH groups, condensation, and decarbonylation [14,15]. Catalyst selection is crucial in the HDO upgrading process. While noble metal catalysts exhibit high activity, economic constraints often lead to the consideration of transition metal catalysts such as NiMo or CoMo [12,16].

The acidity of the catalyst is also a significant factor in HDO reactions. During HDO reactions, Lewis acids primarily adsorb oxygen-containing compounds and Brønsted acids activate hydrogen to react with adsorbed oxygen species. It should be noted that excessive acidity may accelerate coke formation. Cokes hinder the removal of adsorbed oxygen and retard catalyst regeneration. On the other hand, insufficient acidity may impede the proper adsorption of oxygen, thus reducing HDO reactivity [17].

To address the problems associated with BPO when used alone, various methods have been proposed to blend BPO with conventional fuels, such as diesel. However, unlike diesel, which is a non-polar liquid, BPO is a polar liquid, primarily composed of oxygenated compounds that do not form stable mixtures with the hydrocarbon compounds in diesel. This incompatibility presents challenges for effective blending and utilization [18].

In terms of reaction temperature, HDO reactions using precious metal catalysts typically occur at temperatures exceeding 200 °C (Supplementary Information S1). However, zeolite catalysts have been reported to facilitate reactions below this threshold, while alumina catalysts operate effectively within a higher temperature range of 300–500 °C. Furthermore, carbon-based supports have demonstrated improved HDO reactivity when compared to alumina, zeolite, and zirconia-based catalysts. Among carbon-supported noble metal catalysts, the order of hydrogenation activity is Ru/C > Pd/C > Pt/C. For zirconia-supported catalysts, those containing Ru exhibit superior HDO and hydrogenation activity at both high and low temperatures, and they have high reactivity towards guaiacol.

The conversion rates for guaiacol have been reported as 88% for Pd-WO$_x$/γ-Al$_2$O$_3$ and 90% for Pt/H-MFI-90. Such results indicate that phenol exhibits moderate reactivity in model reactions; however, following non-model reactions involving crude BPO, the resulting oil contained elevated levels of phenolic compounds, along with increased concentrations of aromatic and aliphatic hydrocarbons. Transition metal catalysts, including nickel (Ni), cobalt (Co), and molybdenum (Mo) in both single and mixed metal forms, as well as their sulfides and phosphides, have been also investigated (Supplementary Information S2). Generally, Ni outperforms Co in the conversion rates of guaiacol and anisole, demonstrating significant reactivity with acidic supports. Mixed metals such as NiMo, along with their sulfides and phosphides, have proven effective for oxygen removal. In contrast to the carbon-supported noble metal catalysts, transition metal catalysts typically employ alumina as a support material. This choice has shown higher effectiveness in oxygen removal compared to carbon, zeolite, zirconia, and silica supports. Alumina-based catalysts exhibit good performance not only in decarboxylation, decarbonylation, and hydrogenation reactions but also in esterification; however, they demonstrate lower reactivity toward phenolic compounds.

This study aims to investigate HDO reactivity and mechanisms of crude BPO using two types of commercially available alumina-based transition metal catalysts. The two catalysts used have the same bimetals (Ni and Mo) but different distributions of acid sites. Furthermore, we will discuss carbon deposition over catalysts and changes in gas composition generated from different HDO reaction conditions. To evaluate the potential for blending HDO-treated BPO (HDO-BPO) with petroleum-derived fractions, we conducted LCO (light cycle oil) soluble tests.

2. Results and Discussion

2.1. Properties of Crude BPO and Fresh Catalysts

The elemental analysis of crude BPO and HDO-BPO were presented in Table 1. The sample was named by the existence of catalysts, HDO reaction temperatures, and HDO reaction times. Three notations of NC (non-catalyst), NM1, and NM2 were used for three different reaction conditions of no catalyst, NM1 catalyst, and NM2 catalyst, respectively. Reaction temperatures and times were followed to label samples. For instance, for the HDO reaction at 250 °C for 6 h in the presence of the NM1 catalyst, the sample was named HDO-NM1-250-6. At first, the sulfur contents were less than 0.1 wt.% for all samples. In terms of nitrogen (N) contents, the initial amount of nitrogen (0.89 wt.%) within crude BPO was not reduced even after HDO treatments. The results showed a slight increase in nitrogen content, at a range of 0.96 to 1.27 wt.%. Here, it is noticeable that the initial oxygen content (20.4 wt.%) within crude BPO was dramatically decreased down to 6.3 wt.% when the NM2 catalyst was used for 6 h of HDO treatment at 300 °C (HDO-NM2-300-6). Overall, the oxygen reduction was improved when the HDO reaction temperature was increased, as well as when the HDO reaction time was extended from 1 h to 6 h.

In Table 2, the qualitative and quantitative analyses of crude BPO are summarized (the compositions were determined by gas chromatography–mass spectrometry (GC-MS) analysis). The GC-MS analysis data without the catalyst are summarized in Supplementary Information S4. The BPO appears to contain 27 different compounds based on two categorizations of alkyl phenols and oxygenated compounds. A significant portion, accounting for 83.6%, is comprised of alkyl phenols (2-methylphenol and 3-methylphenol), and 5.5% is identified as 3-pentadecyl phenol.

Table 1. Elementary analysis of crude BPO and HDO-BPO.

Liquid Sample	N [wt%]	C [wt%]	H [wt%]	S [wt%]	O [wt%]
Crude BPO	0.89	69.7	8.5	<0.1	20.4
HDO-NC-200-6	1.09	72.3	8.4	<0.1	17.2
HDO-NC-250-6	1.046	73.28	8.82	<0.1	16.5
HDO-NM1-200-6	1.08	72.6	8.8	<0.1	16.6
HDO-NM1-250-1	0.96	74.8	8.9	<0.1	15.2
HDO-NM1-250-6	1.16	75.3	9.2	<0.1	13.8
HDO-NM1-300-1	0.97	76.9	9.2	<0.1	12.4
HDO-NM1-300-3	1.02	78.5	9.4	<0.1	10.3
HDO-NM1-300-6	1.27	80	10	<0.1	8.7
HDO-NM2-200-6	1.00	73.3	8.8	<0.1	16
HDO-NM2-250-1	0.97	74.6	8.6	<0.1	15.3
HDO-NM2-250-6	1.11	74.4	9.2	<0.1	15.4
HDO-NM2-300-1	0.99	77.8	9	<0.1	11.6
HDO-NM2-300-3	1.05	82.6	9.7	<0.1	6.6
HDO-NM2-300-6	1.23	82.5	9.9	<0.1	6.3

Table 2. GC-MS analysis of crude BPO.

	Compound Names	Molecular Formulas	Relative Content (%)
1	(Alkyl) phenols		83.6083
	Phenol, 2-methyl-	C_7H_8O	59.1285
	Phenol, 3-methyl-	C_7H_8O	15.4287
	Phenol, 3-pentadecyl-	$C_{21}H_{36}O$	5.4924
	1,4-Benzenediol, 2-methyl-	$C_7H_8O_2$	0.7683
	Phenol, 2,6-dimethoxy-	$C_8H_{10}O_3$	0.6044
	Phenol, 2-methoxy-4-(1-propenyl)-	$C_{10}H_{12}O_2$	0.5282
	Phenol, 3-ethyl-	$C_8H_{10}O$	0.4292
	Phenol, 2,6-dimethoxy-4-(2-propenyl)-	$C_{11}H_{14}O_3$	0.4273
	Phenol, 4-ethyl-2-methoxy-	$C_9H_{12}O_2$	0.3395
	Mequinol	$C_7H_8O_2$	0.1718
	Phenol	C_6H_6O	0.1533
	Phenol, 3-pentyl-	$C_{11}H_{16}O$	0.1367
2	Oxygenated compounds (including acids, excluding phenol))		16.3917
	Benzenemethanol, alpha.-2-propenyl-	$C_{10}H_{12}O$	3.8354
	(2-cyclohexenyl) propargyl oxide	$C_{10}H_{14}O$	3.2222
	1,6-Anhydro-.beta.-D-glucopyranose (levoglucosan)	$C_6H_{10}O_5$	2.4530
	d-Allose	$C_6H_{12}O_6$	1.4433
	2-propyl-2-cyclohexenone	$C_9H_{16}O$	1.1360
	n-Hexadecanoic acid	$C_{16}H_{32}O_2$	0.8975
	9-Octadecenoic acid	$C_{18}H_{34}O_2$	0.7279
	1,2,4-Trimethoxybenzene	$C_9H_{12}O_3$	0.6160
	Propanenitrile, 2-hydroxy-	C_3H_5NO	0.4661
	2,4-Dimethyl-3-(methoxycarbonyl)-5-ethylfuran	$C_8H_{10}O_3$	0.3395
	Valeraldehyde, 2,2-dimethyl-, oxime	$C_7H_{15}NO$	0.3116
	2-Cyclopenten-1-one,2-hydroxy-3-methyl-	$C_6H_8O_2$	0.2997
	17.beta.-Acetoxy-1.alpha.-carboethoxymethyl-5.alpha.-androstan-3-one	$C_{21}H_{32}O_3$	0.2752
	Desaspidinol	$C_{11}H_{14}O_4$	0.1937
	Phenoxyacetamide	$C_8H_9NO_2$	0.1746

The XRF results for the catalysts are presented in Table 3. The two catalysts exhibit differences mainly in the contents of the promoters, nickel (Ni) and molybdenum (Mo). NM1 (NiMo/alumina-1) contains 1.67% Ni and 3.44% Mo (Ni/Mo ratio = 0.49). In contrast, NM2 (NiMo/alumina-2) contains 3.25% Ni and 13.85% Mo (Ni/Mo ratio = 0.24).

Table 3. XRF analysis of HDO catalysts, NM1 and NM2.

	NM1	**NM2**
Component	mass%	mass%
C	3.02	6.73
O	48.4	48.6
Al	41.8	25.8
Si	0.013	0.0196
P	1.59	1.66
Cr	0.0121	-
K	-	0.022
Fe	0.0262	0.017
Ni	1.67	3.25
Ga	0.0047	0.0051
Mo	3.44	13.8
Nb	0.0053	-
W	-	0.104

The NH_3-TPD analysis results for the catalysts are shown in Figure 1 and Table 4. In the literature [19], the desorption temperatures were categorized by three regions: weak acid sites (<200 °C), medium acid sites (200–400 °C), and strong acid sites (>400 °C). NM1 exhibits peaks between 150 and 400 °C, indicating the presence of weak and medium acid sites. In contrast, NM2 demonstrates a variety of peaks from 150 to 1000 °C, suggesting that it possesses weak, medium, and strong acid sites on its surface. The acidity of NM1 was measured at 1.585 mol/g, while for NM2 it was 12.027 mmol/g. The values show that NM2 has approximately eight times higher acidity than NM1.
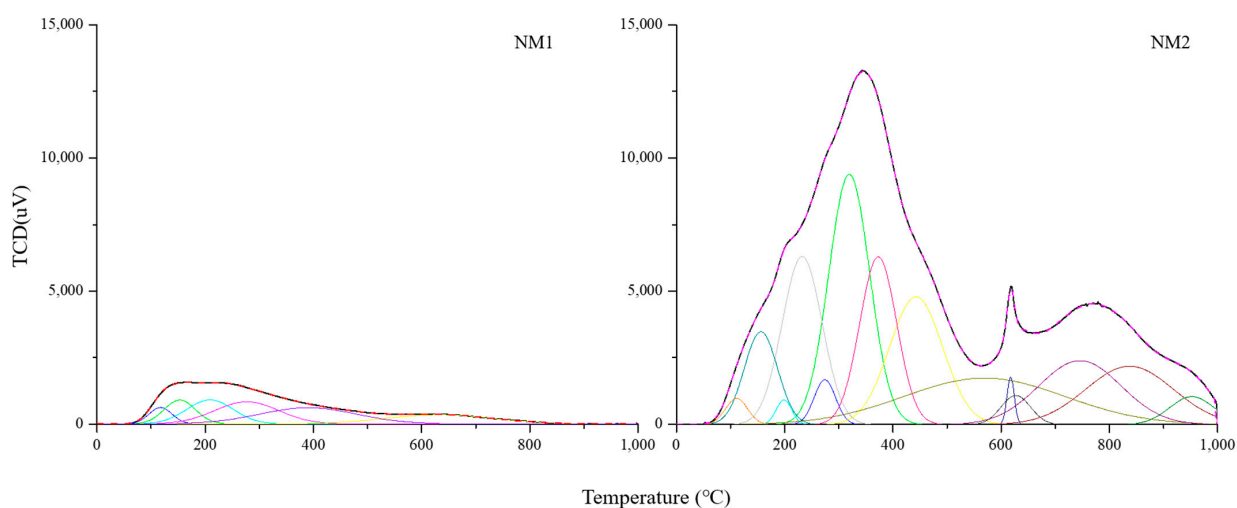
Figure 1. NH_3-TPD curves for NM1 and NM2 catalysts.

Table 4. NH_3-TPD.

	Area	**mmol**	**mmol/g**
NM1	3,663,196	0.162	1.585
NM2	28,484,714	1.260	12.027

It was reported that a higher amount of Ni over Mo inhibits H_2 activation and suppresses HDO activity because MoO_x can cover the outer surface of the Ni, whereas if the Ni/Mo ratio is less than 1, most of the Ni surface cannot be modified by MoO_x and C–C hydrogenation activity and ring hydrogenation activity can be sustained [20]. In another case, Mo acted as a Brønsted acid in the form of Mo-OH, and Ni catalysts with a high MoO_x content exhibited higher activity in HDO reactions [21]. Returning to our case, the Ni/Mo ratios of NM1 and NM2 are below 1, and NM2 shows a wider NH_3-TPD peak area and a greater quantity of NH_3 per unit mass. Based on this, we claim that NM2 possesses higher acidity and a greater number of acid sites, which leads to the enhancement of HDO activity compared to that of NM1.

2.2. HDO Reactivity

The two catalysts (NM1 and NM2) were subjected to reactions at temperatures ranging from 200 to 300 °C, and for reaction times of 1 to 6 h under 60 bar (as shown in Table 1). In the case of the non-catalyzed reaction, the oxygen content was determined to be 17.2 wt% at 200 °C (HDO-NC-200-6) and 16.5 wt% at 250 °C (HDO-NC-250-6). Meanwhile, at 300 °C, rapid gasification of water within BPO occurred, resulting in an increase in the internal pressure of the reactor, which brought safety concerns and subsequently halted the experiment. This infers that the gasification of moisture contributed to the removal of oxygen during the non-catalyzed reactions at 200 °C, as well as at 250 °C.

For NM1 (60 bar for 6 h), the oxygen content was observed to be 16.6 wt% in HDO-NM1-200-6, 13.8 wt% in HDO-NM1-250-6, and 8.7 wt% in HDO-NM1-300-6. This indicates that the oxygen content of HDO-BPO decreased as the reaction temperature increased. When comparing reaction times at 300 °C, the oxygen content was 12.4 wt% in HDO-NM1-300-1, 10.3 wt% in HDO-NM1-300-3, and 8.7 wt% in HDO-NM1-300-6. These showed the successive decreases in oxygen content as the HDO reaction progressed.

Comparing the oxygen contents for NM2-catalysed HDO reactions at various temperatures (60 bar for 6 h), the results were 16.0 wt% in HDO-NM2-200-6, 15.4 wt% in HDO-NM2-250-6, and 6.3 wt% in HDO-NM2-300-6. Even though the decreases in oxygen content were observed as expected, a more sharp decrease was noticed at 300 °C. When comparing reaction times at 250 °C, the oxygen content was 15.3 wt% in HDO-NM2-250-1 and 15.4 wt% in HDO-NM2-250-6. For 300 °C, the oxygen contents were 11.6 wt% in HDO-NM2-300-1, 6.6 wt% in HDO-NM2-300-3, and 6.3 wt% in HDO-NM2-300-6. The progress of deoxygenation was gradually observed at 200 and 250 °C, whereas a sharp decrease was achieved at 300 °C.

It is interesting that NM2 did not show a significant dependence on reaction times up to HDO-NM2-200-6 and HDO-NM2-250-6. Nonetheless, a sharp decrease in oxygen content was achieved for HDO-NM2-300-6. Furthermore, when considering HDO reaction times at 300 °C, NM1 showed gradual decreases in oxygen contents as the reaction progressed: 12.4% in HDO-NM1-300-1, 10.3% in HDO-NM1-300-3, and 8.7% in HDO-NM1-300-6. In an unlikely result, NM2 showed a different reaction progress; that is, 11.6% in HDO-NM2-300-1, 6.6% in HDO-NM2-300-3, and 6.3% in HDO-NM2-300-6. The results indicate that the HDO reaction was almost complete during the first 3 h. Since NM2 demonstrated lower reactivity at 200 °C and 250 °C but high reactivity at 300 °C, it can be presumed that NM2 showed significant dependence upon reaction temperature.

In order to investigate reactivity as a function of reaction temperature, NMR analysis was conducted. Both ^{1}H NMR and ^{13}C NMR results are presented in Figure 2. The ^{1}H NMR results show the gradual removal of internal and terminal double bonds and ether/alcohols within crude BPO when compared before and after HDO treatments in the presence of NM1 and NM2 catalysts (Figure 2a). Each HDO-BPO reaction product was collected after

6 h. With the NM1 catalyst, internal double bonds and ether/alcohols within crude BPO were progressively removed as the HDO reaction temperature increased from 200 °C to 250 °C. In addition, the internal double bonds and ether/alcohols were completely removed at 300 °C. In case of NM2, a small amount of internal double bonds and ether/alcohols remained in reactions up to 250 °C, but were removed completely at 300 °C. It is noticeable that both NM1 and NM2 worked effectively to entirely remove internal double bonds and ether/alcohols at 300 °C. Although there were differences in reactivity between NM1 and NM2, both catalysts demonstrated similar trends in the order of earlier reactivity to remove terminal double bonds, and gradual reactivity to remove internal double bonds and ethers/alcohols, as the HDO reaction temperature increased. The reduction in the amount of double bonds suggests that unsaturated hydrocarbons reacted with hydrogen (H_2) and resulted in the formation of saturated hydrocarbons. The decrease in ether and alcohol content could indicate that oxygenated compounds were effectively removed in advance through the HDO process in the presence of either NM1 or NM2. 3-pentadecyl phenol shows characteristic peaks in the range of 1–2 ppm [22]. Following the HDO reaction, a significant enhancement of the 3-pentadecyl phenol peak was observed, which is consistent with the GC-MS data.
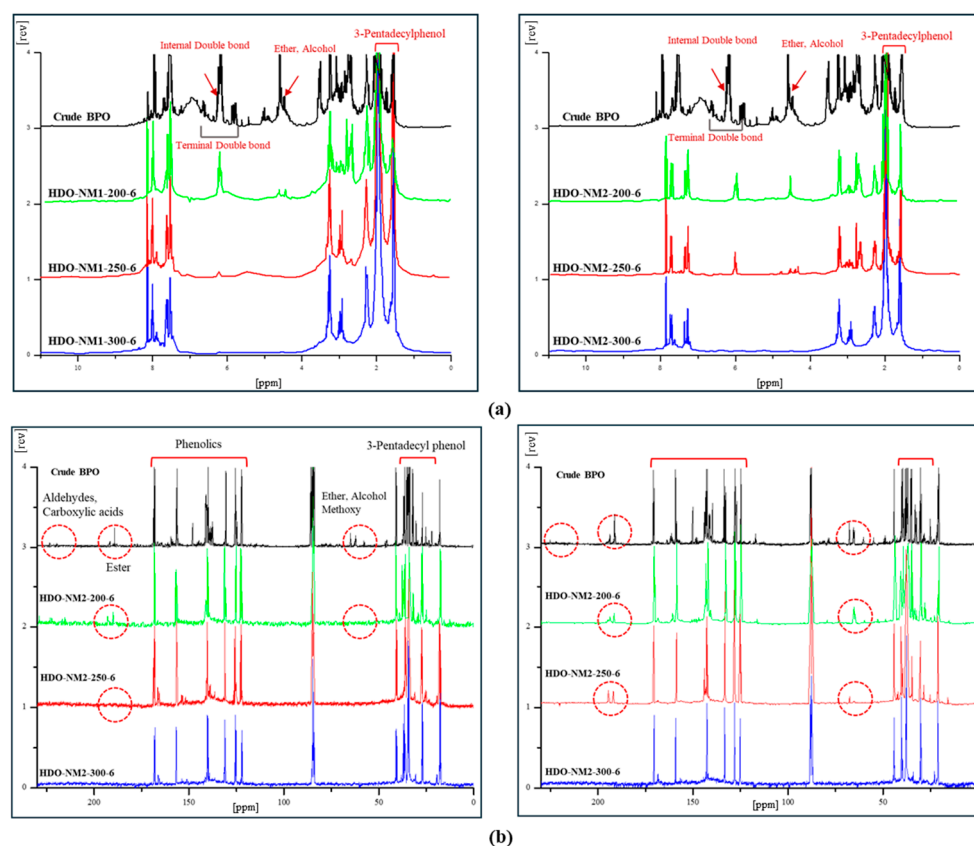

Figure 2. Chemical analyses after HDO treatments in the presence of NM1 and NM2 catalysts using (**a**) ^{1}H NMR spectroscopy and (**b**) ^{13}C NMR spectroscopy.

The ^{13}C NMR analysis results are presented in Figure 2b. Sugar molecules like d-allose and levoglucosan in BPO were decomposed by the HDO reaction over the Ni catalyst at temperatures above 180 °C, transforming into compounds that are not visible in ^{13}C NMR analysis [23]. For NM1 at 200 °C, aldehydes, esters, and alcohols were effectively removed. At 250 °C and 300 °C, all oxygen functional groups except phenolics were eliminated. It should be noted that phenolics still remained after the HDO reaction at 300 °C. In the case of NM2, all oxygen-containing functional groups remained after HDO treatment at

200 °C and 250 °C. Then, at 300 °C all oxygen-containing groups were finally removed, except phenolics. The existence of phenolics is the same as in the NM1 results shown above. As shown in the ^{1}H NMR results, gradual reactivity was shown throughout HDO temperature ranges in NM1, but a sudden reactivity leap was examined at 300 °C in NM2. Overall, both NM1 and NM2 catalysts exhibited the highest reactivity towards aldehydes, a satisfied reactivity over esters, ethers, and alcohols, but the lowest reactivity over phenolics. 3-pentadecyl phenol exhibits peaks in the range of 20–40 ppm [24] in the ^{13}C NMR spectrum. After the HDO reaction, these peaks in BPO were more pronounced compared to crude BPO, further confirming the formation of 3-pentadecyl phenol during HDO.

Density is a key characteristic of fuels. The results of density measurements of HDO-BPO are presented in Figure 3a. The density of crude BPO was found to be 1.0953 g/mL. For NM1, the density was measured to be 1.0598 g/mL at 200 °C, 1.0441 g/mL at 250 °C, and 0.9999 g/mL at 300 °C. The density measurements varied with reaction time, reporting 1.0519 g/mL at 1 h, 1.0395 g/mL at 3 h, and 0.9999 g/mL at 6 h. For NM2, the densities were 1.0646 g/mL at 200 °C, 1.0519 g/mL at 250 °C, and 1.0013 g/mL at 300 °C. The time-specific densities were 1.0503 g/mL at 1 h, 1.0305 g/mL at 3 h, and 1.0013 g/mL at 6 h.
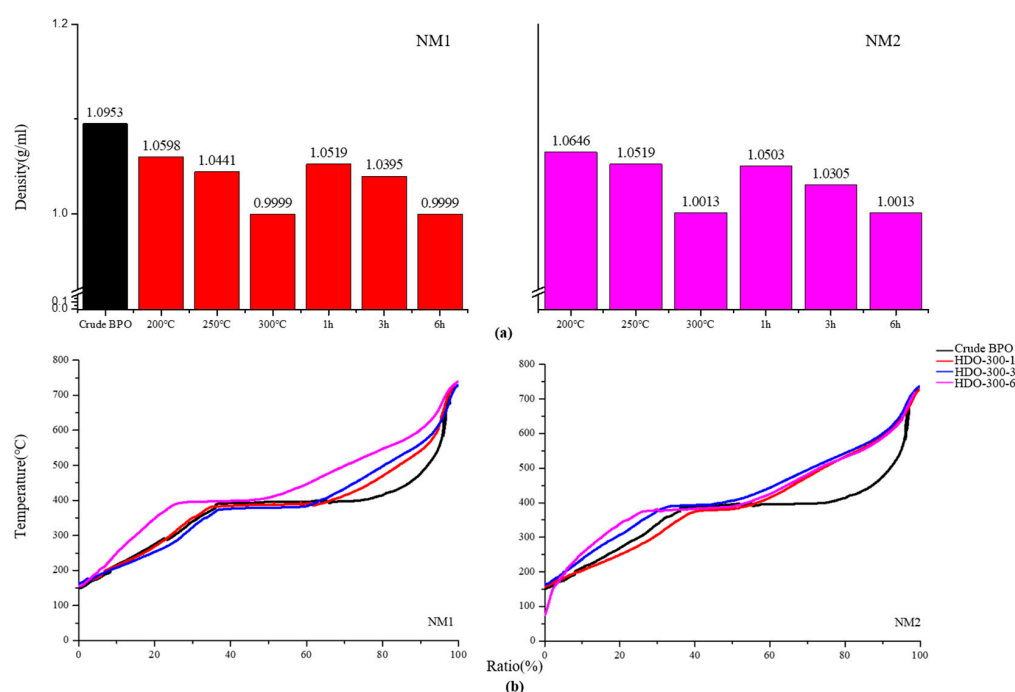

Figure 3. Physical properties of HDO-BPO; (**a**) density data and (**b**) boiling point distribution.

The results of the SIMDIS analysis are presented in Figure 3b. In the case of NM1, the proportion of high boiling point materials increased when compared to crude BPO. The trends observed at 1 h and 3 h were similar, with the proportion of high boiling point materials increasing at 300 °C and 6 h. For NM2, the proportion of high boiling point compounds increased after all HDO reactions, while substances with boiling points ranging from 0 to 400 °C decreased as the reaction time increased. Both NM1 and NM2 showed a trend of decreasing density and increasing boiling points as the HDO reaction increased in temperature and time.

Generally, with longer carbon chains, the space occupied by each molecule increases, and if intermolecular forces are strong, the molecules tend to be closely packed, thereby reducing the distance between them and leading to an increase in density (Figure 4). Two major components in crude BPO are 2-methylphenol and 3-methylphenol (Table 5). Specifically, pentadecyl phenol, which has a longer chain than methyl phenol, occupies

more molecular space (Table 5). Additionally, pentadecyl phenol has a longer non-polar hydrocarbon chain compared to the shorter chain of methyl phenol, resulting in weaker van der Waals forces predominating over hydrogen bonding interactions between molecules, thus increasing the distance between them. For these reasons, it can be inferred that HDO-BPO experiences a decrease in density as the HDO reaction progresses, resulting from the reduction of lighter compounds and the concomitant increase in heavier products due to condensation or additional reactions.
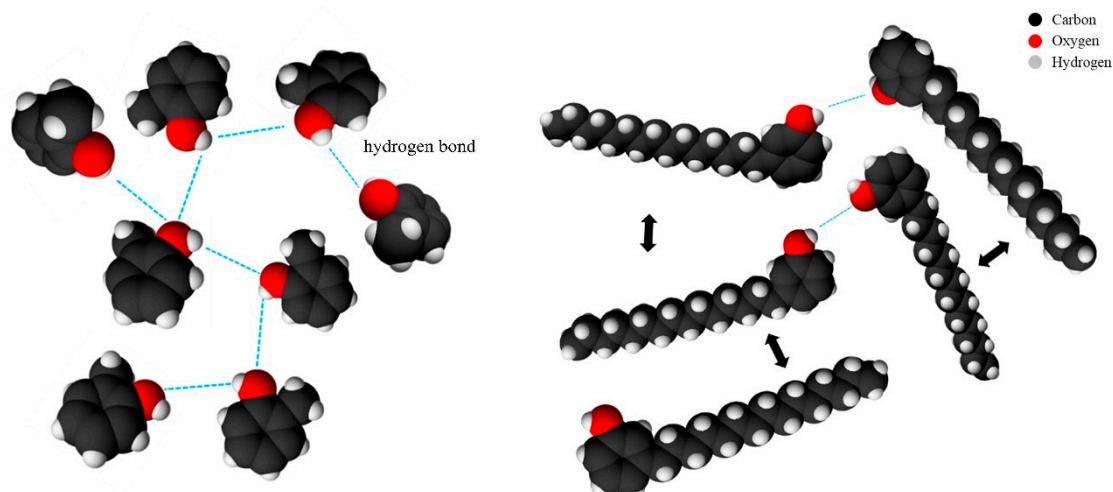

Figure 4. Schematic illustration to show how hydrogen bonds of either smaller molecules or larger molecules affect density reduction.

Table 5. GC-MS analysis of HDO-BPO (60 bar).

Liquid Samples	Relative Content (%)			
	Phenol, 2-Methyl-	Phenol, 3-Methyl-	Phenol, 3-Pentadecyl-	Acetic Acid, 4-Methylphenyl Ester
Crude BPO	59.129	15.429	5.492	-
HDO-NM1-200-6	0.450	1.902	8.617	75.564
HDO-NM1-250-6	0.317	7.430	80.981	-
HDO-NM1-300-1	0.564	0.732	87.615	-
HDO-NM1-300-3	0.502	0.791	80.184	-
HDO-NM1-300-6	0.488	0.875	67.834	-
HDO-NM2-200-6	2.401	5.100	9.214	69.516
HDO-NM2-250-6	2.351	2.411	75.988	-
HDO-NM2-300-1	3.022	1.246	78.898	-
HDO-NM2-300-3	0.971	1.091	53.015	-
HDO-NM2-300-6	0.292	0.978	58.549	-

HDO-BPO exhibits somewhat inferior characteristics compared to coal and petroleum-derived fuels, such as heating values and compatibility with other fuels. To address this limit, subsequent evaluations were conducted to determine the feasibility of mixing the oil with petroleum-derived fractions, including assessments of oil stability and the

hydrocarbon fraction test (HFT). The results related to the LCO solubility, oxygen content, and carbonyl content as a function of reaction conditions are presented in Figure 5. As the degree of the HDO process became more severe, both oxygen and carbonyl contents decreased, while LCO solubility increased. Overall, the carbonyl content was reduced more significantly in NM1-catalysed reactions than in NM2-catalysed reactions. Both HDO-NM1-300-6 and HDO-NM2-300-6 demonstrated over 90% solubility in the blends. The HFT measurements of HDO-BPO confirmed a zero-level detection, indicating a high potential for mixing with petroleum-derived oils.
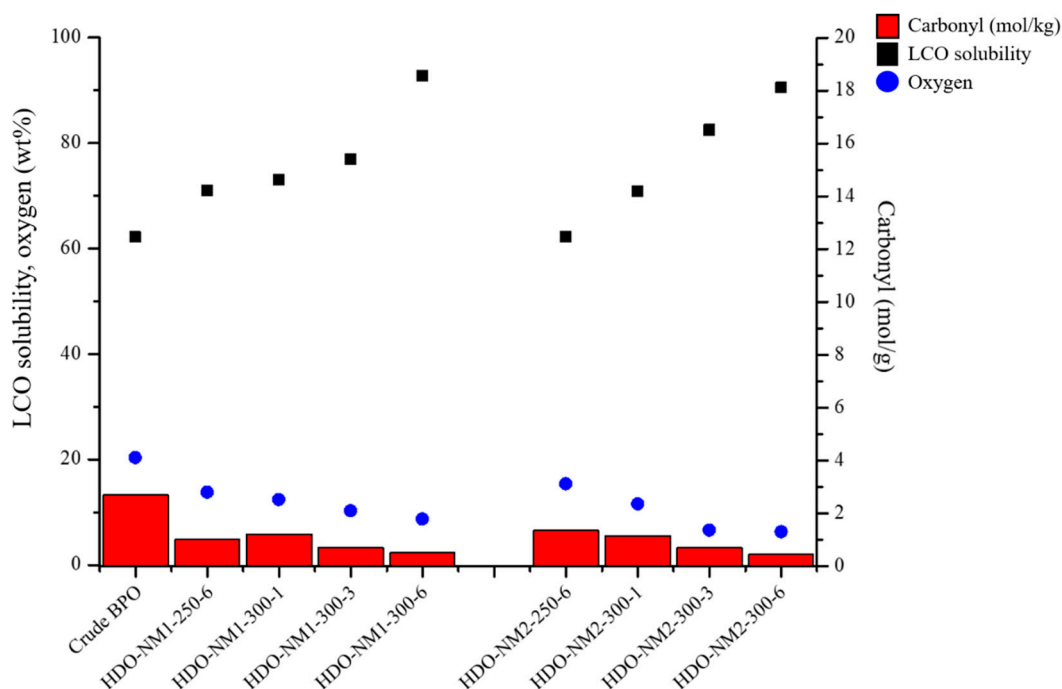
Figure 5. LCO solubility data of HDO-BPO.

2.3. TPO-MS

To investigate the carbon deposition patterns on the catalysts after the reaction, temperature-programmed oxidation–mass spectrometry (TPO-MS) analysis was conducted, as suggested elsewhere [25]. The analysis of spent catalysts was performed following the reactions of HDO-250-6, HDO-300-3, and HDO-300-6, with the results presented in Figure 6. Generally, the CO_2 generation behavior varied similarly across the different reaction temperatures for each catalyst. However, there were distinct differences in CO_2 generation (TPO) behavior between the two catalysts. Specifically, the reaction mechanisms for NM1 and NM2 are clearly different, yet their reaction mechanisms at varying temperatures appear to be quite similar. Commonly, all used catalysts showed an increase in CO_2 production as the reaction temperature rose, with a tendency for the corresponding spectra to shift to higher temperatures. This observation suggests that HDO reactivity becomes more active at elevated temperatures, leading to stronger interactions between the catalyst surface and carbon groups. In terms of specific deposition mechanisms, the NM1 catalyst showed the detection of carboxyl groups solely in the form of WA on its surface. In contrast, the spent NM2 catalyst exhibited the formation of carboxyl (SA and WA) and carboxyl anhydride (CA) groups, as well as lactones (LD and LC) on its surface. Among these, the content of CA was highest, progressively increasing with the reaction temperature (250 °C: 65%, 300 °C: 75%, 350 °C: 84%). This suggests that adjacent carboxyl groups undergo dehydration condensation reactions, resulting in the formation of carboxyl anhydride.
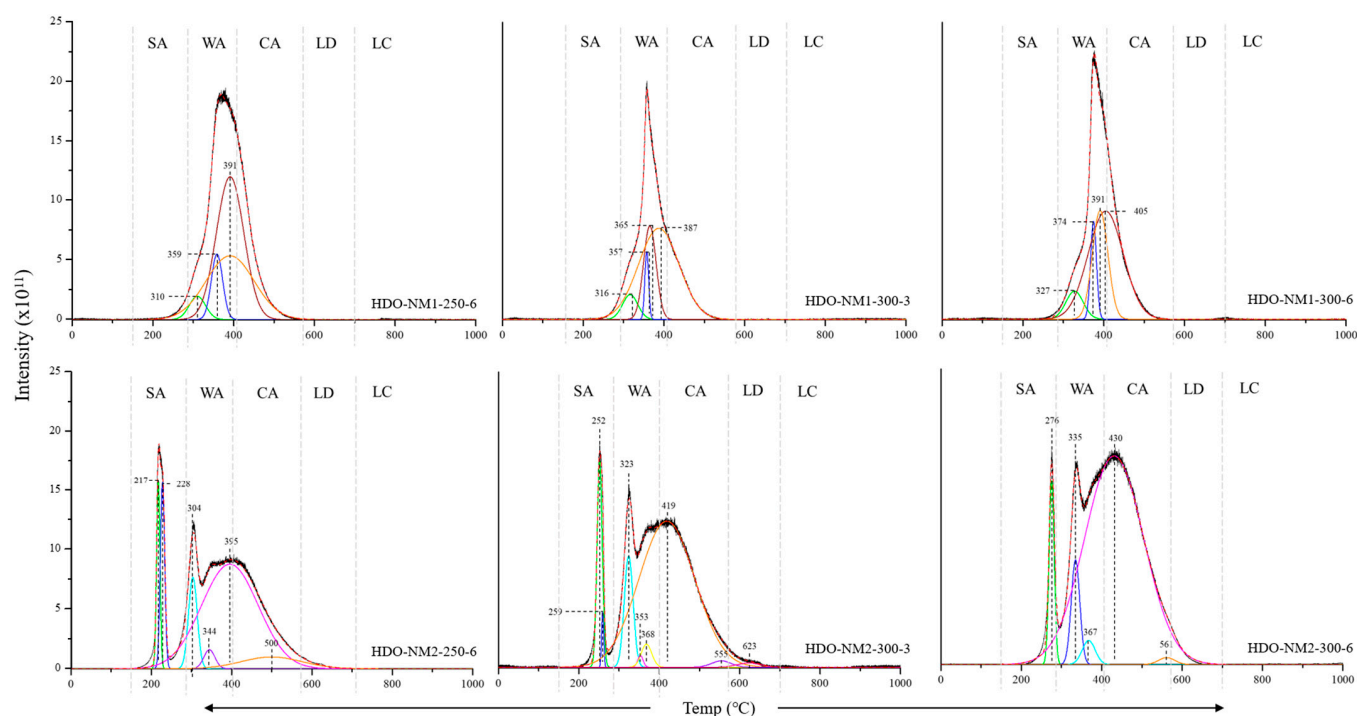
Figure 6. TPO profiles for released CO_2 of spent NM1 and spent NM2 (SA: strongly acidic carboxyls, WA: weakly acidic carboxyls, CA: carboxylic anhydrides, LD and LC: lactones).

2.4. Analysis of Off-Gas

The gases present within the reactor after the HDO reactions were collected and analyzed. The results are presented in Table 6. For both NM1 and NM2, as the reaction temperature and time increased, H_2 levels decreased, while CO_2, CH_4, C_2H_6, and C_3H_8 concentrations increased. Notably, while the amounts of methane, ethane, and propane rose, ethylene and propylene were not significantly detected in the off-gas. In the case of H_2, a marked decrease was observed for NM2 at 300 °C. The composition of the off-gas suggests several possible reactions. The CO_2 generated through decarboxylation is likely converted to CO via a water–gas shift reaction ($CO_2 + H_2 \leftrightarrow CO + H_2O$), followed by methanation ($CO + 3H_2 \leftrightarrow CH_4 + H_2O$), leading to the formation of methane [26,27].

Based on these results, several possible pathways are presented in Figure 7. Two major components in crude BPO are 2-methylphenol and 3-methylphenol (Table 5). It is also noticeable that the amount of 3-pentadecylphenol is about 8%. After HDO treatments at 200 °C for 6 h in the presence of either NM1 or NM2, two major products were acetic acid and 4-methylphenyl ester (4-tolyl acetate). Nevertheless, this component was not detected in our GC-MS analysis later when HDO treatments were performed at 250 and 300 °C in the presence of both NM1 and NM2 catalysts. In specific, reaction times (1–6 h) at 250 and 300 °C did not provide any clues as to whether the reaction begins from methyl phenols, generates acetic acid and 4-methylphenyl ester, and finally terminates to produce 3-pentadecyl phenol. In other words, the reaction of Figure 7(b) does not occur, but the reverse reaction of Figure 7(a) may occur because steam (H_2O) can react with acetic acid and 4-methylphenyl ester to form methyl phenols [28]. If this is true, then this pathway to generate 3-pentadecyl phenol should be proposed, such that it may be generated from a certain supply of C_7 alkyls to generate 3-methyl phenol. It can be persuadable if the HDO reaction and hydrogenation could "partly" generate C_7 alkyls. Figure 7(c) presents an HDO reaction and hydrogenation pathway from 3-methyl phenol [29]. Unfortunately, we have no evidence to support this hypothesis. Nonetheless, the pathway of Figure 7(c) was proposed to generate 3-pentadecyl phenol through the serial reactions of HDO of 3-methyl phenol

to toluene, hydrogenation of toluene to methyl cyclohexane, and ring opening of methyl cyclohexane to C_7 alkyl. Returning to Table 5, it is clear that the existence of 3-pentadecyl phenol is dominant when HDO treatments are performed at 250 and 300 °C. This is also supported by ^{13}C NMR (Figure 2). Even though it is complicated to generate 3-pentadecyl phenol reaction pathways, methyl phenols may be converted to C_7 alkyls. Therefore, it looks as if there are some correlations in how C_{15} has selectively (and dominantly) survived, because methyl phenols have a methyl group (C_1) and partly converted methyl phenols would be C_7 alkyls. The C_{15} can be formed by one C_1 and two C_7 alkyls. Of course, further study into these mechanisms would be needed to verify this hypothesis, with the model chemicals in our system of methyl phenols, acetic acid, 4-methylphenyl ester, and 3-pentadecyl phenol. As crude BPO is composed of a lot of chemicals, the HDO reactions were very complicated. Meanwhile, it is particularly interesting that the major product, 3-pentadecyl phenol, has a C_{15} alkyl group. However, as mentioned previously, there are no clues in our work this time. Further experiments would be required to verify this hypothesis. The ^{13}C NMR analysis confirmed the removal of various other oxygen-containing functional groups, including aldehydes, esters, ethers, and alcohols, following the HDO reaction. Thus, while the aldehydes, esters, ether, alcohols were eliminated, it is inferred that ethylene and propylene, generated through cracking reactions facilitated by the catalyst, reacted with methyl phenol (present in the crude BPO) to form 3-pentadecyl phenol. Consequently, olefins such as ethylene and propylene participated in addition reactions under hydrogen conditions, which likely contributed to their minimal detection in the off-gas.

Table 6. Off gas contents after HDO treatments in the presence of NM1 and NM2.

Gas Sample	HDO-NM1-200-6	HDO-NM1-250-6	HDO-NM1-300-1	HDO-NM1-300-3	HDO-NM1-300-6
C6+	0.05	0.05	0.08	0.15	0.27
Hydrogen	92.61	78.18	82.24	76.85	50.95
Carbon dioxide	3.43	9.87	8.32	11.32	24.38
Methane	0.38	4.91	3.52	5.32	13.45
Ethane	0.04	0.73	0.41	0.88	5.27
Ethylene	0.01	0.07	0.05	0.13	0.05
Propane	0.01	0.19	0.14	0.26	1.95
Propylene	0.03	0.12	0.09	0.12	0
Gas Sample	HDO-NM2-200-6	HDO-NM2-250-6	HDO-NM2-300-1	HDO-NM2-300-3	HDO-NM2-300-6
C6+	0.04	0.11	0.15	0.24	0.18
Hydrogen	92.59	86.74	80.76	54.93	50.07
Carbon dioxide	3.69	6.69	9.73	19.88	22.04
Methane	0.62	3.5	4.22	11.43	12.94
Ethane	0.06	0.45	0.8	4.95	6.22
Ethylene	0.01	0.02	0.06	0.08	0.08
Propane	0.02	0.12	0.22	1.76	2.28
Propylene	0.02	0	0	0.09	0
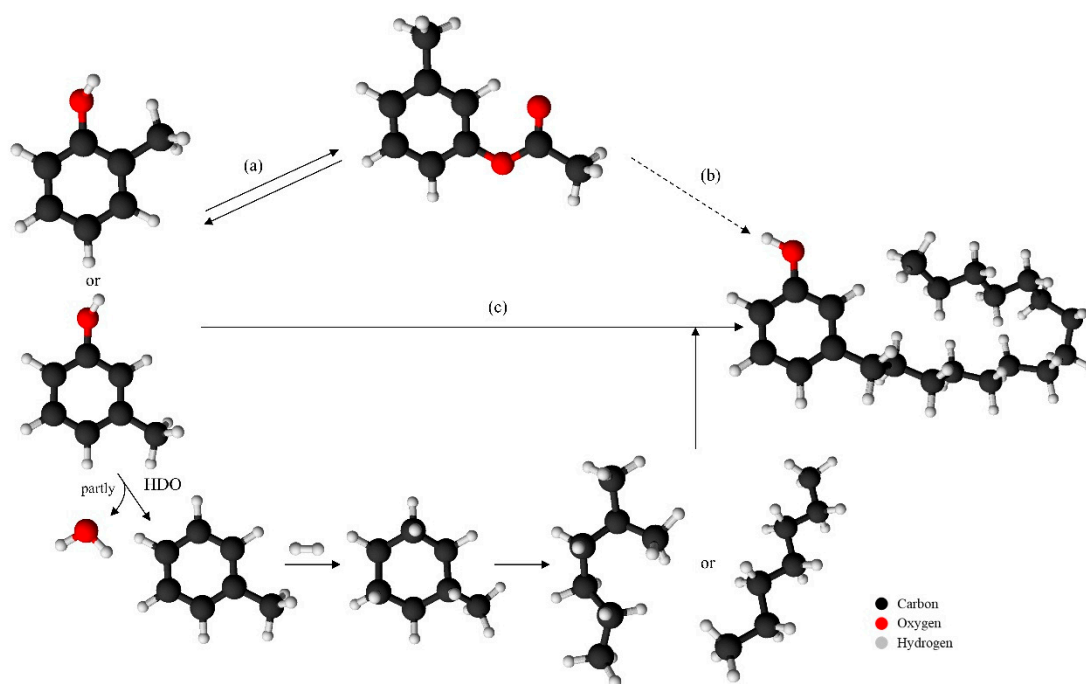
Figure 7. Possible pathways to produce 3-pentadecyl phenol: HDO reaction and hydrogenation of 3-methyl phenol, with ring-opening conversion of methylcyclohexane to alkyl compounds (a) methyl-phenol → 4-methylphenyl ester acetic acid, (b) 4-methylphenyl ester acetic acid → 3-pentadecyl-phenol, (c) methyl-phenol → 3-pentadecyl-phenol.

3. Experimental

3.1. Sulfidation of Catalysts

Two commercial catalysts were used after sulfidation under identical conditions. A controlled rotary tube furnace (TR-1000 series, RX Engineering, Anyang-si, Republic of Korea) was used for sulfidation treatment. Hydrogen sulfide (H_2S) was introduced at a flow rate of 100 mL/min with the temperature being increased from room temperature to 360 °C at the rate of 1 °C/min and maintained for 4 h.

3.2. Hydrodeoxygenation (HDO)

The crude BPO used in this study was a hybrid BPO (clean pine, whole-tree pine, hybrid poplar, and tulip poplar sourced from the Republic of Korea). Crude BPO was provided by a commercial petroleum company located in the Republic Korea. The company also provided commercial catalysts, NM1 and NM2. Since crude BPO is a non-homogeneous mixture, it was placed in an oven (80 °C) and thoroughly mixed prior to the HDO reactions. HDO reactions were performed after loading 30 g of BPO and 3 g of catalyst (weight ratio of 10:1) into a batch reactor (Model 1803-02-Alloy600, Ilhae Systems, Daejeon, Republic of Korea). The reference HDO reactions were arbitrarily determined and set to a temperature of 200 °C, hydrogen pressure of 60 bar, and reaction time of 6 h. Then, the HDO reactions were examined under various conditions of temperature (250 °C and 300 °C) and reaction time (1 and 3 h).

3.3. Characterization of HDO-Treated BP-Oils and Spent Catalysts

After each reaction, HDO-BPO, spent catalysts, and off-gases were analyzed. In most cases, HDO-BPO contained water and needed pre-treatment before characterization. The pre-treatment is as follows. HDO-BPO was kept at 40 °C and centrifuged at 4500 rpm for 15 min. If a layer of water formed either in the upper or lower portions, a syringe was used to separate the water and some oil. In cases where a water layer was present in the

middle layer, the oil was recovered up to the water layer using a syringe, and additional water was removed by tilting the tube to ensure complete separation of the water. After pre-treatment, HDO-BPO underwent serial characterizations: elemental analysis, simulated distillation (SIMDIS), gas chromatography–mass spectrometry (GC-MS), ^{13}C nuclear magnetic resonance (NMR), ^{1}H NMR, and stability evaluation techniques. The spent catalysts were analyzed using ammonia temperature-programmed desorption (NH_3-TPD) and temperature-programmed oxidation–mass spectrometry (TPO-MS) analysis. For the off-gas and elemental analysis measurements, gas chromatography with nitrogen chemiluminescence detection (GC-NCD) was performed.

3.3.1. Elementary Analysis

The elemental composition was analyzed using an Automatic Elemental Analyzer (FLASH 2000, Thermo Fisher Scientific, Waltham, MA, USA). The samples were combusted at approximately 1800 °C, after which the resultant gases were reduced in the reaction chamber. The gases then traversed through a gas chromatography (GC) column, where they were separated based on their respective migration rates and subsequently detected using a thermal conductivity detector (TCD).

3.3.2. SIMDIS

To determine the boiling point distribution of HDO-BPO, a SIMDIS analysis was conducted using an AC Simdis Analyzer (HT750 from PAC, Bethlehem, PA, USA), covering a temperature range of 0 to 800 °C. An Agilent 7890GC (Agilent Technologies, Santa Clara, CA, USA) instrument equipped with a flame ionization detector (FID) and electronic pneumatic control (EPC) was utilized, ensuring high reproducibility. Instrument control was performed using Agilent Chemstation software (E.02.02).

3.3.3. GC-MS

To analyze the composition of HDO-BPO, six case samples (60 bar, same conditions of 200 °C for 6 h; 250 °C for 6 h; 300 °C for 1 h; 300 °C for 3 h; and 300 °C for 6 h) along with the feed were dissolved in methanol. The analysis was performed using an Agilent 6890N GC-MS (Agilent Technologies) instrument equipped with a capillary column (HP-5MS, 5% Phenyl Methyl Siloxane). The oven temperature was increased up to 320 °C, and the measurement was conducted under a helium flow rate of 1.0 mL/min for a duration of 60 min. Only compounds with a quality score of 95% or higher from the GC-MS analysis were specified and integrated. Quantitative concentrations were calculated as the percentage of a specific signal to this sum of integrals.

3.3.4. ^{13}C NMR and ^{1}H NMR

^{13}C NMR analysis was utilized to obtain information regarding the structural characteristics and functional groups of the oil. Measurements were conducted at room temperature using a Bruker (Billerica, MA, USA) AMX-500 spectrometer operating at a frequency of 125 MHz. Meanwhile, ^{1}H NMR analysis was conducted using the same instrument as the ^{13}C NMR analysis, operating at a frequency of 500 MHz. The oil samples (30 mg) were dissolved in 0.5 mL of $CDCl_3$. This optimized the parameters of ^{1}H NMR experiments (AQ (acquisition time) = 4.52 s, d1 (relaxation delay) = 4 s) and C NMR (AQ = 2.9 s, D1 = 10 s).

3.3.5. Light Cycle Oil Solubility

A light cycle oil (LCO) solubility test was conducted according to ASTM E3146 standards [30]. After measuring the weight of the centrifuge tube, a mixture of 95% LCO and 5% HDO-BPO was added to the tube. The tube was then placed in an oven at 60 °C for 1 h and thoroughly shaken. After centrifugation, the supernatant was carefully collected

and separated as an HFT (hydrocarbon fraction test) sample. A pre-determined amount of pentane was added to the remaining tube, and the mixture was shaken for cleaning before centrifugation. The supernatant was then collected, and this washing process was repeated twice, after which the pentane was discarded. The tube was placed back in the oven and kept at 60 °C for 1 h to remove the residual pentane. Finally, the weight of the tube was measured, and the content of the precipitate was assessed after 72 h.

3.3.6. NH_3-TPD

To compare the acid site distributions of the fresh catalyst, NH_3-TPD analysis was performed using the BELCAT II-1 (MicrotracBEL, Osaka, Japan) catalyst characterization system. A 0.1 g sample of the catalyst was dried at 150 °C for 1 h under a helium flow of 30 mL/min to remove moisture. Following this, ammonia (5 vol% NH_3/He) was introduced at a flow rate of 30 mL/min for 1 h to facilitate ammonia adsorption. The catalyst was purged in a nitrogen atmosphere for 1 h. Subsequently, the temperature was increased at a rate of 10 °C/min to approximately 1000 °C to desorb ammonia, which was detected using a MS detector.

3.3.7. XRF

X-ray fluorescence (XRF) analysis from boron (B) to uranium (U) was performed using the Rigaku ZSX Primus IV (Rigaku, Cedar Park, TX, USA) instrument.

3.3.8. TPO-MS

To identify the oxygen-containing functional groups deposited on the spent catalyst, temperature-programmed oxidation (TPO) analysis was conducted. The analysis was performed using the TR-1000 series beads adsorption/desorption test system in conjunction with the BELCAT (Huizhou, China) II Catalyst Analyzer and MASS. Among the ten cases examined, three cases (250 °C for 6 h; 300 °C for 3 h; and 300 °C for 6 h) were selected for analysis of the NM1 and NM2 spent catalysts. For the sample preparation, the spent catalysts were thoroughly washed with toluene and then dried in a vacuum oven at 80 °C for 12 h. After washing and drying, 0.2 g of the spent catalyst was measured and heated at a rate of 5 °C/min to 1000 °C under conditions of an air flow rate of 30 mL/min for CO_2 analysis.

3.3.9. GC-NCD

To assess the nitrogen content (NH_3) in the off-gas, gas chromatography with a nitrogen chemiluminescence detector (GC-NCD) was employed. The NCD detector, known for its high selectivity towards nitrogen compounds, is widely applied in the quantitative analysis of heavy oil and heavy gas oil. The analysis utilized an Agilent 6890N GC-MS (Agilent Technologies) instrument equipped with a capillary column (HP-5MS, 5% phenyl methyl siloxane).

4. Conclusions

HDO-BPO was evaluated in the presence of two commercial alumina-supported transition metal catalysts, NM1 and NM2. Both NM1 and NM2 catalysts removed oxygenated compounds effectively from crude BPO through an HDO upgrading reaction. The results showed a significant reduction in oxygen content, a shift toward higher density, and an increase in boiling point for HDO-BPO. This study revealed that NM2, with higher acidity, exhibited superior HDO reactivity compared to NM1, leading to faster reaction completion and greater oxygen removal at higher temperatures. The analysis of the off-gas composition suggests that decarboxylation, water–gas shift, and methanation reactions are significant processes occurring during the HDO reaction. The HFT results also highlight the potential

for blending HDO-BPO with petroleum-derived fractions. If HDO-BPO shows a favorable compatibility with petroleum fuels, its applications could be wider. Nevertheless, further research is recommended to optimize the HDO process parameters, such as catalyst selection, reaction conditions, and feedstock pre-treatment, to enhance the conversion efficiency and produce high-quality biofuels suitable for blending with conventional fuels.

Supplementary Materials: The following supporting information can be downloaded at: https://www.mdpi.com/article/10.3390/catal15010006/s1. Refs. [31–102] are cited in Supplementary Materials.

Author Contributions: Conceptualization, D.-J.S and J.B.L.; methodology, Y.-J.K.; software, H.-R.C., S.-Y.K. and G.-E.K.; validation, Y.-D.P.; formal analysis, J.-C.A.; investigation, K.O.; resources, G.-E.K., G.-H.K., D.-J.S. and J.-I.P.; data curation, J.B.L.; writing—original draft preparation, D.-J.S. and J.B.L.; writing—review and editing, K.O. and J.-I.P.; visualization, D.-J.S. and J.B.L.; supervision, J.-I.P.; project administration, J.-I.P. All authors have read and agreed to the published version of the manuscript.

Data Availability Statement: The data presented in this study are available on request from the corresponding author.

Conflicts of Interest: The authors declare no conflicts of interest.

References

1. Inayat, A.; Ahmed, A.; Tariq, R.; Waris, A.; Jamil, F.; Ahmed, S.F.; Ghenai, C.; Park, Y.-K. Techno-economical evaluation of bio-oil production via biomass fast pyrolysis process: A review. *Front. Energy Res.* **2022**, *9*, 770355. [CrossRef]

2. Mussatto, S.I.; Yamakawa, C.K.; van der Maas, L.; Dragone, G. New trends in bioprocesses for lignocellulosic biomass and CO_2 utilization. *Renew. Sustain. Energy Rev.* **2021**, *152*, 111620. [CrossRef]

3. Wang, F.; Harindintwali, J.D.; Yuan, Z.; Wang, M.; Wang, F.; Li, S.; Yin, Z.; Huang, L.; Fu, Y.; Li, L. Technologies and perspectives for achieving carbon neutrality. *Innovation* **2021**, *2*, 4. [CrossRef] [PubMed]

4. Hu, X.; Gholizadeh, M. Progress of the applications of bio-oil. *Renew. Sustain. Energy Rev.* **2020**, *134*, 110124. [CrossRef]

5. Winjobi, O.; Shonnard, D.R.; Bar-Ziv, E.; Zhou, W. Life cycle greenhouse gas emissions of bio-oil from two-step torrefaction and fast pyrolysis of pine. *Biofuels Bioprod. Biorefining* **2016**, *10*, 576–588. [CrossRef]

6. Mohan, D.; Pittman, C.U., Jr.; Steele, P.H. Pyrolysis of wood/biomass for bio-oil: A critical review. *Energy Fuels* **2006**, *20*, 848–889. [CrossRef]

7. Guedes, R.E.; Luna, A.S.; Torres, A.R. Operating parameters for bio-oil production in biomass pyrolysis: A review. *J. Anal. Appl. Pyrolysis* **2018**, *129*, 134–149. [CrossRef]

8. Gea, S.; Hutapea, Y.A.; Piliang, A.F.R.; Pulungan, A.N.; Rahayu, R.; Layla, J.; Tikoalu, A.D.; Wijaya, K.; Saputri, W.D. A comprehensive review of experimental parameters in bio-oil upgrading from pyrolysis of biomass to biofuel through catalytic hydrodeoxygenation. *BioEnergy Res.* **2023**, *16*, 325–347. [CrossRef]

9. Xiu, S.; Shahbazi, A. Bio-oil production and upgrading research: A review. *Renew. Sustain. Energy Rev.* **2012**, *16*, 4406–4414. [CrossRef]

10. Zhang, Q.; Chang, J.; Wang, T.; Xu, Y. Review of biomass pyrolysis oil properties and upgrading research. *Energy Convers. Manag.* **2007**, *48*, 87–92. [CrossRef]

11. Routray, K.; Barnett, K.J.; Huber, G.W. Hydrodeoxygenation of pyrolysis oils. *Energy Technol.* **2017**, *5*, 80–93. [CrossRef]

12. Zhang, L.; Liu, R.; Yin, R.; Mei, Y. Upgrading of bio-oil from biomass fast pyrolysis in China: A review. *Renew. Sustain. Energy Rev.* **2013**, *24*, 66–72. [CrossRef]

13. Gollakota, A.R.; Reddy, M.; Subramanyam, M.D.; Kishore, N. A review on the upgradation techniques of pyrolysis oil. *Renew. Sustain. Energy Rev.* **2016**, *58*, 1543–1568. [CrossRef]

14. Lee, H.; Kim, Y.-M.; Lee, I.-G.; Jeon, J.-K.; Jung, S.-C.; Chung, J.D.; Choi, W.G.; Park, Y.-K. Recent advances in the catalytic hydrodeoxygenation of bio-oil. *Korean J. Chem. Eng.* **2016**, *33*, 3299–3315. [CrossRef]

15. Attia, M.; Farag, S.; Chaouki, J. Upgrading of oils from biomass and waste: Catalytic hydrodeoxygenation. *Catalysts* **2020**, *10*, 1381. [CrossRef]

16. Wang, Y.; He, T.; Liu, K.; Wu, J.; Fang, Y. From biomass to advanced bio-fuel by catalytic pyrolysis/hydro-processing: Hydrodeoxygenation of bio-oil derived from biomass catalytic pyrolysis. *Bioresour. Technol.* **2012**, *108*, 280–284. [CrossRef] [PubMed]

17. He, Z.; Wang, X. Required catalytic properties for alkane production from carboxylic acids: Hydrodeoxygenation of acetic acid. *J. Energy Chem.* **2013**, *22*, 883–894. [CrossRef]

18. Martin, J.A.; Mullen, C.A.; Boateng, A.A. Maximizing the stability of pyrolysis oil/diesel fuel emulsions. *Energy Fuels* **2014**, *28*, 5918–5929. [CrossRef]

19. Su, X.; An, P.; Gao, J.; Wang, R.; Zhang, Y.; Li, X.; Zhao, Y.; Liu, Y.; Ma, X.; Sun, M. Selective catalytic hydrogenation of naphthalene to tetralin over a Ni-Mo/Al2O3 catalyst. *Chin. J. Chem. Eng.* **2020**, *28*, 2566–2576. [CrossRef]

20. Yang, F.; Libretto, N.J.; Komarneni, M.R.; Zhou, W.; Miller, J.T.; Zhu, X.; Resasco, D.E. Enhancement of m-cresol hydrodeoxygenation selectivity on Ni catalysts by surface decoration of MoO x species. *ACS Catal.* **2019**, *9*, 7791–7800. [CrossRef]

21. Kukushkin, R.; Bulavchenko, O.; Kaichev, V.; Yakovlev, V. Influence of Mo on catalytic activity of Ni-based catalysts in hydrodeoxygenation of esters. *Appl. Catal. B Environ.* **2015**, *163*, 531–538. [CrossRef]

22. ChemicalBook. Available online: https://www.chemicalbook.com/SpectrumEN_501-24-6_1HNMR.htm (accessed on 15 December 2024).

23. Boscagli, C.; Raffelt, K.; Grunwaldt, J.D. Reactivity of platform molecules in pyrolysis oil and in water during hydrotreatment over nickel and ruthenium catalysts. *Biomass Bioenergy* **2017**, *106*, 63–73. [CrossRef]

24. ChemicalBook. Available online: https://www.chemicalbook.com/SpectrumEN_501-24-6_13CNMR.htm (accessed on 15 December 2024).

25. Li, N.; Ma, X.; Zha, Q.; Kim, K.; Chen, Y.; Song, C. Maximizing the number of oxygen-containing functional groups on activated carbon by using ammonium persulfate and improving the temperature-programmed desorption characterization of carbon surface chemistry. *Carbon* **2011**, *49*, 5002–5013. [CrossRef]

26. Mortensen, P.M.; Grunwaldt, J.-D.; Jensen, P.A.; Knudsen, K.; Jensen, A.D. A review of catalytic upgrading of bio-oil to engine fuels. *Appl. Catal. A Gen.* **2011**, *407*, 1–19. [CrossRef]

27. Onarheim, K.; Hannula, I.; Solantausta, Y. Hydrogen enhanced biofuels for transport via fast pyrolysis of biomass: A conceptual assessment. *Energy* **2020**, *199*, 117337. [CrossRef]

28. Kumar, A.; Kumar, A.; Biswas, B.; Kumar, J.; Yenumala, S.R.; Bhaskar, T. Hydrodeoxygenation of m-Cresol over Ru based catalysts: Influence of catalyst support on m-Cresol conversion and methylcyclohexane selectivity. *Renew. Energy* **2020**, *151*, 687–697. [CrossRef]

29. Piegsa, A.; Korth, W.; Demir, F.; Jess, A. Hydrogenation and ring opening of aromatic and naphthenic hydrocarbons over noble metal (Ir, Pt, Rh)/Al 2 O 3 catalysts. *Catal. Lett.* **2012**, *142*, 531–540. [CrossRef]

30. *ASTM E3146*; Standard Test Method for Determination of Carbonyls in Pyrolysis Bio-Oils by Potentiometric Titration. ASTM International: West Conshohocken, PA, USA, 2024.

31. Elliott, D.C.; Hart, T.R.; Neuenschwander, G.G.; Rotness, L.J.; Zacher, A.H. Catalytic hydroprocessing of biomass fast pyrolysis bio-oil to produce hydrocarbon products. *Environ. Prog. Sustain. Energy* **2009**, *28*, 441–449. [CrossRef]

32. Chaiwat, W.; Gunawan, R.; Gholizadeh, M.; Li, X.; Lievens, C.; Hu, X.; Wang, Y.; Mourant, D.; Rossiter, A.; Bromly, J. Upgrading of bio-oil into advanced biofuels and chemicals. Part II. Importance of holdup of heavy species during the hydrotreatment of bio-oil in a continuous packed-bed catalytic reactor. *Fuel* **2013**, *112*, 302–310. [CrossRef]

33. Oh, S.; Hwang, H.; Choi, H.S.; Choi, J.W. Investigation of chemical modifications of micro-and macromolecules in bio-oil during hydrodeoxygenation with Pd/C catalyst in supercritical ethanol. *Chemosphere* **2014**, *117*, 806–814. [CrossRef] [PubMed]

34. Wildschut, J.; Mahfud, F.H.; Venderbosch, R.H.; Heeres, H.J. Hydrotreatment of fast pyrolysis oil using heterogeneous noble-metal catalysts. *Ind. Eng. Chem. Res.* **2009**, *48*, 10324–10334. [CrossRef]

35. Venderbosch, R.H.; Ardiyanti, A.R.; Wildschut, J.; Oasmaa, A.; Heeres, H. Stabilization of biomass-derived pyrolysis oils. *J. Chem. Technol. Biotechnol.* **2010**, *85*, 674–686. [CrossRef]

36. Chen, L.; Zhu, Y.; Zheng, H.; Zhang, C.; Zhang, B.; Li, Y. Aqueous-phase hydrodeoxygenation of carboxylic acids to alcohols or alkanes over supported Ru catalysts. *J. Mol. Catal. A Chem.* **2011**, *351*, 217–227. [CrossRef]

37. Liu, C.; Shao, Z.; Xiao, Z.; Liang, C. Hydrodeoxygenation of benzofuran over activated carbon supported Pt, Pd, and Pt–Pd catalysts. *React. Kinet. Mech. Catal.* **2012**, *107*, 393–404. [CrossRef]

38. Cordero-Lanzac, T.; Palos, R.; Arandes, J.M.; Castaño, P.; Rodríguez-Mirasol, J.; Cordero, T.; Bilbao, J. Stability of an acid activated carbon based bifunctional catalyst for the raw bio-oil hydrodeoxygenation. *Appl. Catal. B Environ.* **2017**, *203*, 389–399. [CrossRef]

39. Madsen, A.T.; Christensen, C.H.; Fehrmann, R.; Riisager, A. Hydrodeoxygenation of waste fat for diesel production: Study on model feed with Pt/alumina catalyst. *Fuel* **2011**, *90*, 3433–3438. [CrossRef]

40. Payormhorm, J.; Kangvansaichol, K.; Reubroycharoen, P.; Kuchonthara, P.; Hinchiranan, N. Pt/Al$_2$O$_3$-catalytic deoxygenation for upgrading of Leucaena leucocephala-pyrolysis oil. *Bioresour. Technol.* **2013**, *139*, 128–135. [CrossRef] [PubMed]

41. Ying, X.; Tiejun, W.; Longlong, M.; Guanyi, C. Upgrading of fast pyrolysis liquid fuel from biomass over Ru/γ-Al$_2$O$_3$ catalyst. *Energy Convers. Manag.* **2012**, *55*, 172–177. [CrossRef]

42. Hong, Y.-K.; Lee, D.-W.; Eom, H.-J.; Lee, K.-Y. The catalytic activity of Pd/WOx/γ-Al$_2$O$_3$ for hydrodeoxygenation of guaiacol. *Appl. Catal. B Environ.* **2014**, *150*, 438–445. [CrossRef]

43. Zheng, Y.; Wang, J.; Li, D.; Liu, C.; Lu, Y.; Lin, X.; Zheng, Z. Highly efficient catalytic pyrolysis of biomass vapors upgraded into jet fuel range hydrocarbon-rich bio-oil over a bimetallic Pt–Ni/γ-Al$_2$O$_3$ catalyst. *Int. J. Hydrogen Energy* **2021**, *46*, 27922–27940. [CrossRef]

44. Zhang, C.; Xing, J.; Song, L.; Xin, H.; Lin, S.; Xing, L.; Li, X. Aqueous-phase hydrodeoxygenation of lignin monomer eugenol: Influence of Si/Al ratio of HZSM-5 on catalytic performances. *Catal. Today* **2014**, *234*, 145–152. [CrossRef]

45. Hellinger, M.; Carvalho, H.W.; Baier, S.; Wang, D.; Kleist, W.; Grunwaldt, J.-D. Catalytic hydrodeoxygenation of guaiacol over platinum supported on metal oxides and zeolites. *Appl. Catal. A Gen.* **2015**, *490*, 181–192. [CrossRef]

46. Wang, Y.; Fang, Y.; He, T.; Hu, H.; Wu, J. Hydrodeoxygenation of dibenzofuran over noble metal supported on mesoporous zeolite. *Catal. Commun.* **2011**, *12*, 1201–1205. [CrossRef]

47. Gutierrez, A.; Kaila, R.K.; Honkela, M.L.; Slioor, R.; Krause, A.O.I. Hydrodeoxygenation of guaiacol on noble metal catalysts. *Catal. Today* **2009**, *147*, 239–246. [CrossRef]

48. Ohta, H.; Feng, B.; Kobayashi, H.; Hara, K.; Fukuoka, A. Selective hydrodeoxygenation of lignin-related 4-propylphenol into n-propylbenzene in water by Pt-Re/ZrO2 catalysts. *Catal. Today* **2014**, *234*, 139–144. [CrossRef]

49. Sheu, Y.-H.E.; Anthony, R.G.; Soltes, E.J. Kinetic studies of upgrading pine pyrolytic oil by hydrotreatment. *Fuel Process. Technol.* **1988**, *19*, 31–50. [CrossRef]

50. Lu, J.; Heyden, A. Theoretical investigation of the reaction mechanism of the hydrodeoxygenation of guaiacol over a Ru (0 0 0 1) model surface. *J. Catal.* **2015**, *321*, 39–50. [CrossRef]

51. Guo, C.; Rao, K.T.V.; Yuan, Z.; He, S.Q.; Rohani, S.; Xu, C.C. Hydrodeoxygenation of fast pyrolysis oil with novel activated carbon-supported NiP and CoP catalysts. *Chem. Eng. Sci.* **2018**, *178*, 248–259. [CrossRef]

52. Duan, D.; Zhang, Y.; Lei, H.; Villota, E.; Ruan, R. Renewable jet-fuel range hydrocarbons production from co-pyrolysis of lignin and soapstock with the activated carbon catalyst. *Waste Manag.* **2019**, *88*, 1–9. [CrossRef]

53. Duan, D.; Zhang, Y.; Lei, H.; Qian, M.; Villota, E.; Wang, C.; Wang, Y.; Ruan, R. A novel production of phase-divided jet-fuel-range hydrocarbons and phenol-enriched chemicals from catalytic co-pyrolysis of lignocellulosic biomass with low-density polyethylene over carbon catalysts. *Sustain. Energy Fuels* **2020**, *4*, 3687–3700. [CrossRef]

54. Mateo, W.; Lei, H.; Villota, E.; Qian, M.; Zhao, Y.; Huo, E.; Zhang, Q.; Lin, X.; Wang, C.; Huang, Z. Synthesis and characterization of sulfonated activated carbon as a catalyst for bio-jet fuel production from biomass and waste plastics. *Bioresour. Technol.* **2020**, *297*, 122411. [CrossRef]

55. Lin, X.; Lei, H.; Huo, E.; Qian, M.; Mateo, W.; Zhang, Q.; Zhao, Y.; Wang, C.; Villota, E. Enhancing jet fuel range hydrocarbons production from catalytic co-pyrolysis of Douglas fir and low-density polyethylene over bifunctional activated carbon catalysts. *Energy Convers. Manag.* **2020**, *211*, 112757. [CrossRef]

56. Sepúlveda, C.; Leiva, K.; García, R.; Radovic, L.; Ghampson, I.; DeSisto, W.; Fierro, J.G.; Escalona, N. Hydrodeoxygenation of 2-methoxyphenol over Mo2N catalysts supported on activated carbons. *Catal. Today* **2011**, *172*, 232–239. [CrossRef]

57. Echeandia, S.; Arias, P.; Barrio, V.; Pawelec, B.; Fierro, J. Synergy effect in the HDO of phenol over Ni–W catalysts supported on active carbon: Effect of tungsten precursors. *Appl. Catal. B Environ.* **2010**, *101*, 1–12. [CrossRef]

58. De la Puente, G.; Gil, A.; Pis, J.; Grange, P. Effects of support surface chemistry in hydrodeoxygenation reactions over CoMo/activated carbon sulfided catalysts. *Langmuir* **1999**, *15*, 5800–5806. [CrossRef]

59. Zhou, M.; Tian, L.; Niu, L.; Li, C.; Xiao, G.; Xiao, R. Upgrading of liquid fuel from fast pyrolysis of biomass over modified Ni/CNT catalysts. *Fuel Process. Technol.* **2014**, *126*, 12–18. [CrossRef]

60. Duan, D.; Feng, Z.; Zhang, Y.; Zhou, T.; Xu, Z.; Wang, Q.; Zhao, Y.; Wang, C.; Ruan, R. Corncob pyrolysis: Improvement in hydrocarbon group types distribution of bio oil from co-catalysis over HZSM-5 and activated carbon. *Waste Manag.* **2022**, *141*, 8–15. [CrossRef] [PubMed]

61. Ausavasukhi, A.; Huang, Y.; To, A.T.; Sooknoi, T.; Resasco, D.E. Hydrodeoxygenation of m-cresol over gallium-modified beta zeolite catalysts. *J. Catal.* **2012**, *290*, 90–100. [CrossRef]

62. Veses, A.; Puértolas, B.; Callén, M.; García, T. Catalytic upgrading of biomass derived pyrolysis vapors over metal-loaded ZSM-5 zeolites: Effect of different metal cations on the bio-oil final properties. *Microporous Mesoporous Mater.* **2015**, *209*, 189–196. [CrossRef]

63. Qian, M.; Lei, H.; Villota, E.; Zhao, Y.; Huo, E.; Wang, C.; Mateo, W.; Zou, R. Enhanced production of renewable aromatic hydrocarbons for jet-fuel from softwood biomass and plastic waste using hierarchical ZSM-5 modified with lignin-assisted re-assembly. *Energy Convers. Manag.* **2021**, *236*, 114020. [CrossRef]

64. Kumar, P.; Yenumala, S.R.; Maity, S.K.; Shee, D. Kinetics of hydrodeoxygenation of stearic acid using supported nickel catalysts: Effects of supports. *Appl. Catal. A Gen.* **2014**, *471*, 28–38. [CrossRef]

65. Ayodele, O.; Farouk, H.U.; Mohammed, J.; Uemura, Y.; Daud, W.M.A.W. Hydrodeoxygenation of oleic acid into n-and iso-paraffin biofuel using zeolite supported fluoro-oxalate modified molybdenum catalyst: Kinetics study. *J. Taiwan Inst. Chem. Eng.* **2015**, *50*, 142–152. [CrossRef]

66. Bu, Q.; Lei, H.; Zacher, A.H.; Wang, L.; Ren, S.; Liang, J.; Wei, Y.; Liu, Y.; Tang, J.; Zhang, Q. A review of catalytic hydrodeoxygenation of lignin-derived phenols from biomass pyrolysis. *Bioresour. Technol.* **2012**, *124*, 470–477. [CrossRef]

67. Nava, R.; Pawelec, B.; Castaño, P.; Álvarez-Galván, M.; Loricera, C.; Fierro, J. Upgrading of bio-liquids on different mesoporous silica-supported CoMo catalysts. *Appl. Catal. B Environ.* **2009**, *92*, 154–167. [CrossRef]

68. Romero, Y.; Richard, F.; Brunet, S. Hydrodeoxygenation of 2-ethylphenol as a model compound of bio-crude over sulfided Mo-based catalysts: Promoting effect and reaction mechanism. *Appl. Catal. B Environ.* **2010**, *98*, 213–223. [CrossRef]

69. Etienne, L.; Bernard, D. Study of the hydrodeoxygenation of carbonyl, carboxylic and guaiacyl groups over sulfided CoMo/γ-Al 2 O 3 and NiMo/γ-Al 2 O 3 catalysts. I. Catalytic reaction schemes. *Appl. Catal. A Gen.* **1994**, *109*, 77–96.

70. Wandas, R.; Surygala, J.; Śliwka, E. Conversion of cresols and naphthalene in the hydroprocessing of three-component model mixtures simulating fast pyrolysis tars. *Fuel* **1996**, *75*, 687–694. [CrossRef]

71. Massoth, F.; Politzer, P.; Concha, M.; Murray, J.; Jakowski, J.; Simons, J. Catalytic hydrodeoxygenation of methyl-substituted phenols: Correlations of kinetic parameters with molecular properties. *J. Phys. Chem. B* **2006**, *110*, 14283–14291. [CrossRef] [PubMed]

72. Zhao, C.; Kasakov, S.; He, J.; Lercher, J.A. Comparison of kinetics, activity and stability of Ni/HZSM-5 and Ni/Al$_2$O$_3$-HZSM-5 for phenol hydrodeoxygenation. *J. Catal.* **2012**, *296*, 12–23. [CrossRef]

73. Jin, S.; Xiao, Z.; Li, C.; Chen, X.; Wang, L.; Xing, J.; Li, W.; Liang, C. Catalytic hydrodeoxygenation of anisole as lignin model compound over supported nickel catalysts. *Catal. Today* **2014**, *234*, 125–132. [CrossRef]

74. Yang, Y.; Ochoa-Hernández, C.; Pizarro, P.; Coronado, J.M.; Serrano, D.P. Effect of metal–support interaction on the selective hydrodeoxygenation of anisole to aromatics over Ni-based catalysts. *Appl. Catal. B Environ.* **2014**, *145*, 91–100. [CrossRef]

75. Ryymin, E.-M.; Honkela, M.L.; Viljava, T.-R.; Krause, A.O.I. Competitive reactions and mechanisms in the simultaneous HDO of phenol and methyl heptanoate over sulphided NiMo/γ-Al$_2$O$_3$. *Appl. Catal. A Gen.* **2010**, *389*, 114–121. [CrossRef]

76. Rocha, J.; Luengo, C.; Snape, C. Hydrodeoxygenation of oils from cellulose in single and two-stage hydropyrolysis. *Renew. Energy* **1996**, *9*, 950–953. [CrossRef]

77. Šimáček, P.; Kubička, D.; Šebor, G.; Pospíšil, M. Fuel properties of hydroprocessed rapeseed oil. *Fuel* **2010**, *89*, 611–615. [CrossRef]

78. Pham, T.T.; Lobban, L.L.; Resasco, D.E.; Mallinson, R.G. Hydrogenation and Hydrodeoxygenation of 2-methyl-2-pentenal on supported metal catalysts. *J. Catal.* **2009**, *266*, 9–14. [CrossRef]

79. Kwon, K.C.; Mayfield, H.; Marolla, T.; Nichols, B.; Mashburn, M. Catalytic deoxygenation of liquid biomass for hydrocarbon fuels. *Renew. Energy* **2011**, *36*, 907–915. [CrossRef]

80. Xu, Y.; Wang, T.; Ma, L.; Zhang, Q.; Liang, W. Upgrading of the liquid fuel from fast pyrolysis of biomass over MoNi/γ-Al$_2$O$_3$ catalysts. *Appl. Energy* **2010**, *87*, 2886–2891. [CrossRef]

81. Wang, Y.; Lin, H.; Zheng, Y. Hydrotreatment of lignocellulosic biomass derived oil using a sulfided NiMo/γ-Al$_2$O$_3$ catalyst. *Catal. Sci. Technol.* **2014**, *4*, 109–119. [CrossRef]

82. Ardiyanti, A.; Khromova, S.; Venderbosch, R.; Yakovlev, V.; Heeres, H. Catalytic hydrotreatment of fast-pyrolysis oil using non-sulfided bimetallic Ni-Cu catalysts on a δ-Al$_2$O$_3$ support. *Appl. Catal. B Environ.* **2012**, *117*, 105–117. [CrossRef]

83. Le, T.A.; Ly, H.V.; Kim, J.; Kim, S.-S.; Choi, J.H.; Woo, H.-C.; Othman, M.R. Hydrodeoxygenation of 2-furyl methyl ketone as a model compound in bio-oil from pyrolysis of Saccharina Japonica Alga in fixed-bed reactor. *Chem. Eng. J.* **2014**, *250*, 157–163. [CrossRef]

84. Mortensen, P.M. Catalytic Conversion of Bio-Oil to Fuel for Transportation. Ph.D. Thesis, Technical University of Denmark, Lyngby, Denmark, 2013.

85. Zhao, H.; Li, D.; Bui, P.; Oyama, S. Hydrodeoxygenation of guaiacol as model compound for pyrolysis oil on transition metal phosphide hydroprocessing catalysts. *Appl. Catal. A Gen.* **2011**, *391*, 305–310. [CrossRef]

86. Iino, A.; Cho, A.; Takagaki, A.; Kikuchi, R.; Oyama, S.T. Kinetic studies of hydrodeoxygenation of 2-methyltetrahydrofuran on a Ni2P/SiO2 catalyst at medium pressure. *J. Catal.* **2014**, *311*, 17–27. [CrossRef]

87. Cheng, S.; Wei, L.; Julson, J.; Rabnawaz, M. Upgrading pyrolysis bio-oil through hydrodeoxygenation (HDO) using non-sulfided Fe-Co/SiO2 catalyst. *Energy Convers. Manag.* **2017**, *150*, 331–342. [CrossRef]

88. Leiva, K.; Martinez, N.; Sepulveda, C.; García, R.; Jiménez, C.; Laurenti, D.; Vrinat, M.; Geantet, C.; Fierro, J.; Ghampson, I. Hydrodeoxygenation of 2-methoxyphenol over different Re active phases supported on SiO2 catalysts. *Appl. Catal. A Gen.* **2015**, *490*, 71–79. [CrossRef]

89. Furimsky, E. Catalytic hydrodeoxygenation. *Appl. Catal. A Gen.* **2000**, *199*, 147–190. [CrossRef]

90. Wang, W.; Yang, Y.; Luo, H.; Hu, T.; Liu, W. Amorphous Co–Mo–B catalyst with high activity for the hydrodeoxygenation of bio-oil. *Catal. Commun.* **2011**, *12*, 436–440. [CrossRef]

91. Baldauf, W.; Balfanz, U.; Rupp, M. Upgrading of flash pyrolysis oil and utilization in refineries. *Biomass Bioenergy* **1994**, *7*, 237–244. [CrossRef]

92. Yoosuk, B.; Tumnantong, D.; Prasassarakich, P. Unsupported MoS2 and CoMoS2 catalysts for hydrodeoxygenation of phenol. *Chem. Eng. Sci.* **2012**, *79*, 1–7. [CrossRef]

93. Apaydin-Varol, E.; Pütün, E.; Pütün, A.E. Slow pyrolysis of pistachio shell. *Fuel* **2007**, *86*, 1892–1899. [CrossRef]

94. Grilc, M.; Veryasov, G.; Likozar, B.; Jesih, A.; Levec, J. Hydrodeoxygenation of solvolysed lignocellulosic biomass by unsupported MoS2, MoO2, Mo2C and WS2 catalysts. *Appl. Catal. B Environ.* **2015**, *163*, 467–477. [CrossRef]

95. Yunquan, Y.; Gangsheng, T.; Smith, K.J.; Tye, C.T. Hydrodeoxygenation of phenolic model compounds over MoS2 catalysts with different structures. *Chin. J. Chem. Eng.* **2008**, *16*, 733–739.

96. Sankaranarayanan, T.M.; Berenguer, A.; Ochoa-Hernández, C.; Moreno, I.; Jana, P.; Coronado, J.M.; Serrano, D.P.; Pizarro, P. Hydrodeoxygenation of anisole as bio-oil model compound over supported Ni and Co catalysts: Effect of metal and support properties. *Catal. Today* **2015**, *243*, 163–172. [CrossRef]

97. Wang, W.-Y.; Yang, Y.-Q.; Bao, J.-G.; Luo, H.-A. Characterization and catalytic properties of Ni–Mo–B amorphous catalysts for phenol hydrodeoxygenation. *Catal. Commun.* **2009**, *11*, 100–105. [CrossRef]

98. Mante, O.D.; Dayton, D.C.; Gabrielsen, J.; Ammitzboll, N.L.; Barbee, D.; Verdier, S.; Wang, K. Integration of catalytic fast pyrolysis and hydroprocessing: A pathway to refinery intermediates and "drop-in" fuels from biomass. *Green Chem.* **2016**, *18*, 6123–6135. [CrossRef]

99. Wang, W.; Zhang, K.; Qiao, Z.; Li, L.; Liu, P.; Yang, Y. Hydrodeoxygenation of p-cresol on unsupported Ni–W–Mo–S catalysts prepared by one step hydrothermal method. *Catal. Commun.* **2014**, *56*, 17–22. [CrossRef]

100. Jęczmionek, Ł.; Porzycka-Semczuk, K. Hydrodeoxygenation, decarboxylation and decarbonylation reactions while co-processing vegetable oils over NiMo hydrotreatment catalyst. Part II: Thermal effects–Experimental results. *Fuel* **2014**, *128*, 296–301. [CrossRef]

101. Popov, A.; Kondratieva, E.; Gilson, J.-P.; Mariey, L.; Travert, A.; Maugé, F. IR study of the interaction of phenol with oxides and sulfided CoMo catalysts for bio-fuel hydrodeoxygenation. *Catal. Today* **2011**, *172*, 132–135. [CrossRef]

102. Asphaug, S. *Catalytic Hydrodeoxygenation of Bio-Oils with Supported MoP-Catalysts*; Institutt for Kjemisk Prosessteknologi: Trondheim, Norway, 2013.